SEGMENTATION AND ANALYSIS OF INSULIN GRANULE MEMBRANES IN BETA ISLET CELL ELECTRON MICROGRAPHS

David Nam[1], *Judith Mantell*[2,3], *Dave Bull*[1], *Paul Verkade*[2,3,4,*] *and, Alin Achim*[1*]

[1]Visual Information Laboratory, [2]Wolfson Bioimaging Facility, [3]School of Biochemistry, [4]School of Physiology and Pharmacology. University of Bristol, Bristol, UK. *shared last author

ABSTRACT

Quantification of sub cellular structures is necessary in understanding how cells function. This paper presents a segmentation algorithm for transmission electron microscopy images of insulin granule membranes from beta cells of rat islet of Langerhans. Granules are described as having a dense core and a surrounding halo. We use a mixed vector field convolution snake to segment the granule membranes. We also present a novel contribution to the convergence filter family, which uses an adjustable region of support. The filter is used to verify our segmentation. We calculate pixel error by comparing the membrane areas from our method with a manually defined ground truth. 1300 granules are used in our test and an average area difference of 7.54% is observed.

Index Terms— Transmission electron microscopy, convergence filters, granule segmentation, image processing.

1. INTRODUCTION

Electron microscopes have allowed researchers to observe sub cellular structures at high resolution. With this detail, accurate quantitative analysis may be performed. This allows cellular processes to be described numerically, and eventually leads to better understanding and prediction of cellular functions. It is common for researchers to manually analyze these images to get quantitative information. This can lead to human error, bias, irreproducibility and it is also slow.

Insulin is vital for life, being the only hormone in mammals able to lower blood glucose levels. Disbalance of insulin levels may result in diabetes. The hormone is secreted by beta cells inside islets of Langerhans of the pancreas. After its biosynthesis, insulin is processed and packaged in granules. Typically, insulin granules are described as organelles containing a dense core, surrounded by a halo and an enclosing membrane. Not all granules have this surrounding halo, this being very much dependent on the fixation procedure. In this work, transmission electron microscopy (TEM) images of rat beta cells have been acquired to examine the physical dimensions of their insulin granule membranes. This work is an extension to our work done in [1], where we present an algorithm for granule core segmentation. In high-throughput screening image analysis, image segmentation is the most critical step [2].

A number of approaches for microscopy cell segmentation have been previously described. Normally image thresholding methods, for example Otsu's [3], are used for segmentation. Methods based on watershed transforms [4] and multiscale products [5] have also been proposed. Beta islet TEM images however have many complex structures present and none of these methods is readily applicable to granule membrane segmentation. Recently, an automated method dedicated for the analysis of insulin granules was developed [6]. It was developed for a specific (expensive) software package; Definiens. This methodology should be open source. We present a segmentation algorithm specifically tailored for granule membranes. A mixed vector field convolution (VFC) external force is introduced for a parametric active contour model. The mixed force is designed to attract the contour towards the granule membrane. It also contains a repulsive force to prevent the contour from settling inside the granule core. Each active contour is initialized using the granule core, which was segmented using the method presented in [1]. For some granules the membrane is at the core, hence they do not have a halo. In order to validate our segmentation from the mixed VFC, we developed an adjustable sliding band filter. The filter detects the amount a convergence for a given point within a defined region of support. If the membrane is segmented correctly, its gradient flow will converge towards its center.

The reminder of the paper is described as follows: Section 2 reviews the VFC force and describes our adjustable sliding band filter. In Section 3 we present our membrane segmentation algorithm. We validate our approach in Section 4 and conclude in Section 5.

2. THEORETICAL PRELIMINARIES

The TEM image, along with the core segmentations and an image of the TEM segmented by a level set active contour (BW) — both presented in [1]— are used as inputs for the algorithm. The membrane segmentation algorithm proceeds through the following steps: morphological operations, sampling, VFC snake and verification (Fig. 1).

2.1. Vector Field Convolution

Active contours are often used in image segmentation methods; they are based on partial differential equations. The basic idea in active contour segmentation models is to evolve a curve, subject to constraints from a given image, in order to detect objects in that image. In [7] contours are represented by a parametric curve, $c(s) = [x(s), y(s)]^T$; $s =\in [0, 1]$. The curve will deform through the image, to minimize the following energy functional [8]:

$$E_{ac} = \int_0^1 [\frac{1}{2}(\alpha \left|c'(s)\right|^2 + \beta \left|c''(s)\right|^2) + E_{ext}(c(s))]ds. \quad (1)$$

The two constants α and β are weighting parameters, which represent the amount of smoothness and tautness of the contour, respectively. The term with α and β represent the internal energy of the contour. E_{ext} denotes the external energy; this is determined by image features. VFC snakes are a class of parametric snakes which use the VFC force as the external force for the contour. This external force is calculated by convolving each component of a discrete vector field kernel with an edge map. The vector field kernel is defined as follows,

$$k(x, y) = m(x, y)n(x, y), \quad (2)$$

where $m(x, y)$ is the magnitude of the vector at (x, y) and $n(x, y)$ is the unit vector pointing to the kernel origin $(0, 0)$, $n(x, y) = [-\frac{x}{r_{ac}}, -\frac{y}{r_{ac}}]$, $r_{ac} = \sqrt{(x^2 + y^2)}$. At the origin where $r_{ac} = 0$, $n(0, 0) = [0, 0]$. This type of kernel has the property that a free particle placed in the field will move towards the origin. The value of $m(x, y)$ should always be positive and decreasing farther away from the origin. The magnitude function used is described as,

$$m(x, y) = (r_{ac} + \epsilon_{ac})^{-\gamma} \quad (3)$$

γ is a positive constant used to control the decrease and ϵ_{ac} is a small positive constant to prevent division by zero at the origin [7].

The external VFC force, $f_{vfc}(x, y)$ can be calculated by convolving the discrete vector field kernel with the image edge map, $f_{edge}(x, y)$. At the minima of (1), the contour must satisfy the Euler-Lagrange equation:

$$\alpha c'' - \beta c'''' - \nabla E_{ext}(c) = 0. \quad (4)$$

Where $\alpha c'' - \beta c''''$ is the internal force to control the contour smoothness and tautness, and $f_{vfc}(c) = -\nabla E_{ext}(c)$ is the external force that attracts the contour toward the features of interest. In order to solve (4), $c(s)$ is treated as a function of time t. The solution is obtained at the steady state solution of the gradient descent equation below:

$$\frac{\partial c(s, t)}{\partial t} = \alpha c''(s, t) - \beta c''''(s, t) + f_{vfc}(c(s, t)). \quad (5)$$

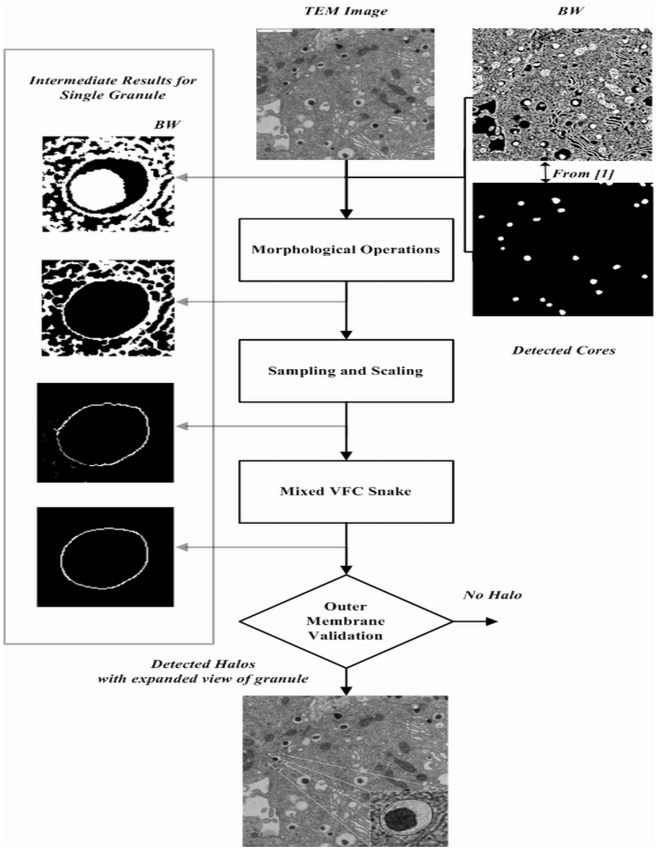

Fig. 1: Flow chart displaying the granule membrane segmentation algorithm using a section of a TEM image.

A solution to (5) can be reached by solving a discretization of s iteratively using a finite difference approach [7]. Since edges on the edge map have the largest values, they will contribute more to $f_{vfc}(x, y)$ than homogeneous regions, therefore the contour will be more attracted towards the edges of the image.

2.2. Adjustable Sliding Band Filter

The sliding band filter is part of the family of convergence filters, which evaluate the degree of convergence of the gradient vectors within its region of support toward a pixel of interest. The degree of convergence is related to the distribution of the directions of the gradient vectors and not to their magnitudes. The convergence index of a gradient vector at a given pixel is defined as the cosine of its orientation with respect to the line connecting the pixel and the pixel of interest,

$$C_{conv}(x, y) = \frac{1}{M} \sum_{(k,l)\in R} cos\theta(k, l). \quad (6)$$

M is the number of points in the filter support region R, θ is the angle between the gradient vector calculated at point (k, l) and the direction of the line that connects points (x, y)

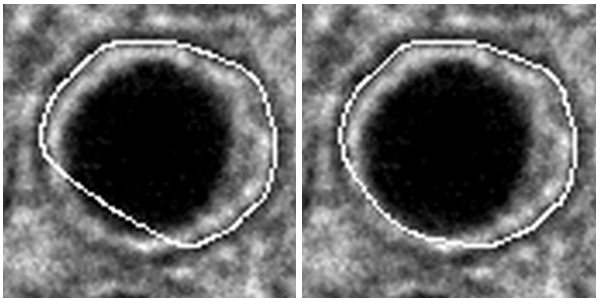

Fig. 2: Segmentation using VFC force from sampled membrane only and mixed VFC force, left and right respectively.

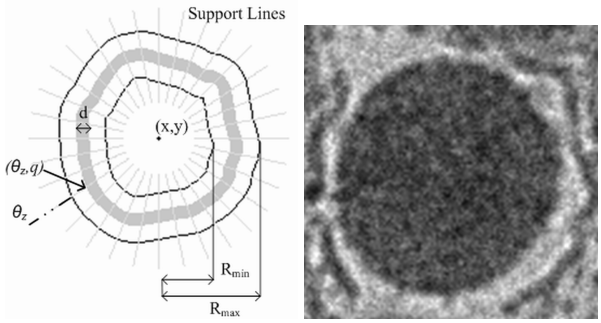

Fig. 3: Support region schematics for adjustable SBF (left), for granule on right.

and (k, l). Several different convergence filters have been proposed: coin filters, iris filters, adaptive ring filters and sliding band filters [9], [10] and [11] respectively. The sliding band filter, [11], [12] has a support region formed by a band of fixed width, whose position is changed in each direction to allow the maximization of the convergence index at each point. Having an annulus shaped support region allows the sliding band filter to detect convex shapes. In our algorithm, the outer radius of the region of support for the sliding band filter would correspond to the farthest membrane point from the center of the membrane, while the inner radius would correspond to the nearest membrane point. While this is sufficient for granules with a circular halo, granules with an elliptical or other non circular halo would have an unnecessarily large region of support. The proposed improvement allows for a more flexible region of support R. R can now be defined as any closed contour. This allows for more flexibility, depending on the application. The improved sliding band filter is defined as:

$$SBF_{adj}(x,y) = \tfrac{1}{N}\textstyle\sum_{z=1}^{N} \\ max(\tfrac{1}{d+1}\textstyle\sum_{q=r-(\frac{d}{2})}^{r+(\frac{d}{2})} CI(z,q)), \quad R_{min}^z \le r \le R_{max}^z \quad (7)$$

where

$$CI(z,q) = cos(\theta_z - \alpha_{cf}(\theta_z, q)) \\ \theta_z = \frac{2\pi}{N}(z-1) \\ \alpha_{cf}(\theta_z, q) = arctan(\frac{\frac{dI(\theta_z,q)}{dx}}{\frac{dI(\theta_z,q)}{dy}}).$$

and I is the intensity (TEM) image, N is the number of support region lines (to sample R) that irradiate from (x,y), d is the band width, r is the position of the band in a line that varies from R_{min}^z to R_{max}^z and CI is the cosine of the angle between the direction that is currently being analyzed θ_z and the image gradient vector direction at location (θ_z, q). Generally, images are redundant, hence the average of the convergence indices on N support region lines can be used to represent C_{conv} if N is sufficiently large [9]. R_{min}^z and R_{max}^z represents the length of the closest and farthest points to (x, y) along support line z respectively.

3. MEMBRANE SEGMENTATION ALGORITHM

The halo segmentation algorithm uses the black and white result, (BW) of the level set active contour and the core segmentations from [1]. The proposed algorithm for granule halo extraction is outlined in Fig. 1. In order to segment the membrane the core is removed from BW, but first dilated by a small amount to ensure that all of the core is removed. Morphological thinning is then applied to BW, to thin the membrane. The granule membrane is then sampled, by projecting outwards from the center of the core until the first non zero pixel is found. This is done for 360 degrees. The result is a close representation of the granule membrane but the membrane may not be connected, due to it not always being smooth. Morphological bridging is used to connect these disjoint pixels. Although at this point the membrane may be fully segmented, some membranes have gaps or are incomplete, hence the VFC snake is used to fill in these gaps. Before this however, the sampled points need to be scaled. Points that make up the largest set of connected components, have a value of 1, points in the second largest set a value of $\frac{1}{2}$, third largest $\frac{1}{3}$ and so on. The granule membrane makes up the majority of the sampled points, hence they are assigned the greatest weight. Other points which are not connected to the membrane are usually objects in the cytoplasm; they are usually small and unconnected to each other therefore should provide less attraction to the snake.

The contour is initialized as a circle within the membrane. The center of the circle is taken as the average of the x and y coordinates of all points of the sampled membrane. The radius is taken as the distance from the center point to the point closest to the center point. The VFC kernel distance is chosen as the average distance of all points from the center point. Large values are used for α and β to encourage a regular shape of the membrane, particularly when filling in gaps. In order to prevent the contour from moving inside the core a mixed external field is proposed. A second external

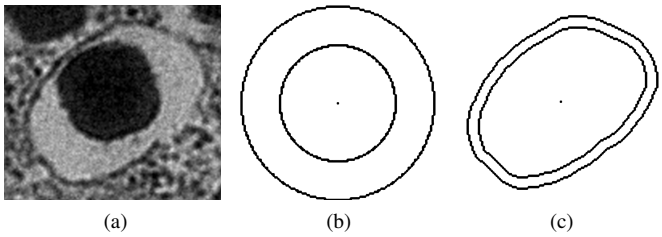

(a) (b) (c)

Fig. 4: Granule with elliptical membrane (a). SBF region of support (b). SBF_{adj} region of support (c).

force is calculated using the negative core border as an edge map, but with the same parameters used to calculate the first force. This produces an external force pushing the contour away from the core. The mixed external force is as follows:

f_{mixed} = $f_{vfc}(x, y)$ from sampled and scaled membrane – if outside of core

f_{mixed} = $f_{vfc}(x, y)$ from core – if inside core

3.1. Membrane Verification

We need a method to evaluate our segmentation because for some granules the membrane is at the core, therefore there is no halo. If under 40% of a membrane is detected, the granule is classified as not having a halo. In order to check for this, the segmented membrane is overlapped with BW. If more than 40% of the membrane is overlapped, the segmentation is kept, otherwise it is omitted. Granules where the membranes are at the core, are surrounded by cytoplasm. This case does not give a continuous smooth border, when compared to granules with a halo. Checking the overlap of the segmentation from the VFC snake and BW can sometimes lead to a false detection of a halo. This can be the case if there are many segmented parts of the cytoplasm surrounding the granule core provide the area for the VFC segmentation to overlap with. As an extra measure to improve the detection accuracy, the improved SBF presented above is employed. The motivation behind it is that if a granule has a surrounding halo, that membrane's gradient flow will converge towards the granule's center. Since only the areas around the granule centers are of interest, only points within 30 pixels from the center points were calculated. Given the result of the VFC snake as $C(x, y)$, the region of support for SBF_{adj} is defined as $R = dilate(C, se)$ where se is a circularly structured element of diameter D_{se}. This creates a band in the shape of C. The size of the region of support is determined by D_{se} and hence by R^n_{min} and R^n_{max} as well. Properly segmented halos will have a peak in the filter magnitude response image, located around the granule centers. To evaluate the strength of each peak the following metric was utilized:

$$PS = \frac{1}{p} \sum_{x_{i=1}}^{p} \frac{(SBF^i_{adj} - avg)}{dist}, \qquad (8)$$

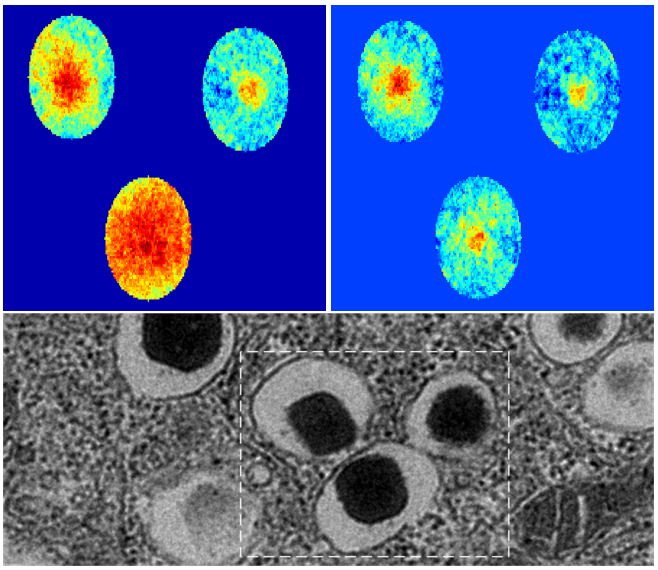

Fig. 5: Filter response from a section of a TEM image. Bottom row shows the TEM image with filter response area indicated by the dashed lines. Response using the SBF (top left), and the response using SBF_{adj} (top right). Notice that the SBF_{adj} has more uniform and focused responses for each granule, despite the membrane shape.

where p is the number of points in which the SBF_{adj} is calculated for each core, SBF^i_{adj} is SBF_{adj} at point x_i, avg is the average SBF_{adj} and $dist$ is the is distance from x_i to the center of the core. If $dist < 1$, $dist = 1$. The metric proposed gives higher values to filter responses with a peak in the center. Granule halo segmentations with a PS smaller than 0.0085 are considered to be incorrect, and the membrane is then determined to be at the core.

4. RESULTS

The TEM images used to test our algorithm were 5000×5000 pixels. Our algorithm is initially applied to five images, two fixed chemically and three fixed using cryofixation. This corresponds to about 1300 granules to be processed. For the VFC snake $\alpha = 20$, $\beta = 20$, $\gamma = 1.1$ and $\triangle t = 0.5$. Within the sliding band filter, $D_{se} = 4$ and $N = 32$. Fig. 2 shows the effects of membrane segmentation using the force from the sampled membrane alone and the mixed VFC force. Fig. 3 shows a granule with a surrounding halo and its corresponding region of support for the adjustable SBF. In Fig. 4 (b), the region of support for the SBF is shown for a granule with an elliptical membrane (a). The region of support for the adjustable SBF on the same granule is shown in Fig. 4 (c), note the larger region of support in (b). Fig. 5 demonstrates the advantages of using the adjustable SBF against the SBF. As a final step the same images were also manually analyzed and the results compared with the automated analysis. In order to

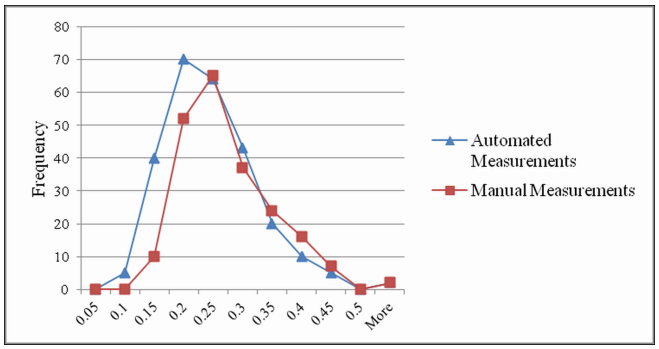

Fig. 6: Granule membrane radii distributions for a TEM image of a chemically fixed Beta Islet cell. The horizontal axis is the radii bins in μm, while the vertical axis is frequency.

Table 1: Beta islet cell granule membrane radii for 5 images, together with manually measured values. M = Mean, SD = Standard Deviation, CF = Chemically fixed, HPF = High pressure fixation.

	Proposed Algorithm		Ground Truth	
	M (μm)	SD(μm)	M (μm)	SD(μm)
CF 1	0.24207	0.08355	0.28139	0.07222
HPF 1	0.23923	0.04915	0.24254	0.04965
CF 2	0.22239	0.07707	0.24986	0.07546
HPF 2	0.16440	0.05917	0.18203	0.05166
HPF 3	0.21631	0.06350	0.21258	0.06141

check the accuracy of our algorithm we compared the average granule membrane areas, with those done manually. The metric used to record granule sizes is a radius of a circle of the same area as the area enclosed by the granule membrane. Fig. 6 shows the distribution of granule membrane sizes of the proposed algorithm and the ground truth. The average granule membrane radii error is 7.54%. Table. 1 summarizes our results on membrane distributions on all five images.

5. CONCLUSION

In this paper we have presented an automatic segmentation approach for the membrane of insulin granules in TEM images of beta islet cells. Portions of the membrane are first sampled from BW using radial projections from the granule core centers. Gaps in the sampled membrane are filled using the VFC snake with a mixed f_{vfc} to prevent the contour from settling within the core. Not all granules have a surrounding halo. To verify our segmentation, we developed an adjustable sliding band filter to determine the convergence around the possible granule membrane. The possible membrane is also overlapped with BW to see how much the segmented membranes match. We validated our method on a set of five images (1300 granules). The pixel error is calculated by comparing the membrane areas from our method with those done manually.

6. REFERENCES

[1] D. Nam, J. Mantell, D. Bull, P. Verkade, and A. Achim, "Active contour based segmentation for electron microscopy images of insulin granule cores," *Engineering in Medicine and Biology Society, EMBC, 2012 Annual International Conference of the IEEE, San Diego, California*, August 2012.

[2] X. Zhou and S.T.C. Wong, "Informatics challenges of high-throughput microscopy," *Signal Processing Magazine, IEEE*, vol. 23, no. 3, pp. 63 –72, May 2006.

[3] N. Otsu, "A threshold selection method from gray-level histograms," *Systems, Man and Cybernetics, IEEE Transactions on*, vol. 9, no. 1, pp. 62 –66, Jan. 1979.

[4] H. Nguyen and Q. Ji, "Shape-driven three-dimensional watersnake segmentation of biological membranes in electron tomography," *Medical Imaging, IEEE Transactions on*, vol. 27, no. 5, pp. 616 –628, May 2008.

[5] J.-C. Olivo-Marin, "Extraction of spots in biological images using multiscale products," *Pattern Recognition*, vol. 35, no. 9, pp. 1989 – 1996, 2002.

[6] E. Fava, J. Dehghany, J. Ouwendijk, A. Müller, A. Niederlein, P. Verkade, M. Meyer-Hermann, and M. Solimena, "Novel standards in the measurement of rat insulin granules combining electron microscopy, high-content image analysis and in silico modelling," *Diabetologia*, vol. 55, pp. 1013–1023, 2012, 10.1007/s00125-011-2438-4.

[7] B. Li and S.T. Acton, "Active contour external force using vector field convolution for image segmentation," *Image Processing, IEEE Transactions on*, vol. 16, no. 8, pp. 2096 –2106, Aug. 2007.

[8] M. Kass, A. Witkin, and D. Terzopoulos, "Snakes: Active contour models," *International Journal of Computer Vision*, vol. 1, no. 4, pp. 321–331, 1988.

[9] H. Kobatake and S. Hashimoto, "Convergence index filter for vector fields," *Image Processing, IEEE Transactions on*, vol. 8, no. 8, pp. 1029 –1038, Aug 1999.

[10] J. Wei, Y. Hagihara, and H. Kobatake, "Detection of rounded opacities on chest radiographs using convergence index filter," *Image Analysis and Processing, 1999. Proceedings. International Conference on*, pp. 757 –761, 1999.

[11] C. Pereira, H. Fernandes, A. Mendonça, and A. Campilho, "Detection of lung nodule candidates in chest radiographs," *Pattern Recognition and Image Analysis*, vol. 4478, pp. 170–177, 2007.

[12] P. Quelhas, M. Marcuzzo, A.M. Mendonca, and A. Campilho, "Cell nuclei and cytoplasm joint segmentation using the sliding band filter," *Medical Imaging, IEEE Transactions on*, vol. 29, no. 8, pp. 1463 –1473, Aug. 2010.